

Directional vortex motion guided by artificially induced mesoscopic potentials.

J. E. Villegas¹, E. M. Gonzalez¹, M. I. Montero², Ivan K. Schuller², and J. L. Vicent¹

¹ Departamento de Física de Materiales, Facultad CC. Físicas, Universidad Complutense, 28040 Madrid (Spain).

² Department of Physics, University of California-San Diego, La Jolla, CA 92093 –0319 (USA).

ABSTRACT.

Rectangular pinning arrays of Ni dots define a potential landscape for vortex motion in Nb films. Magnetotransport experiments in which two in-plane orthogonal electrical currents are injected simultaneously allow selecting the direction and magnitude of the Lorentz force on the vortex-lattice, thus providing the angular dependence of the vortex motion.

The background dissipation depends on angle at low magnetic fields, which is progressively smeared out with increasing field. The periodic potential locks in the vortex motion along channeling directions. Because of this, vortex-lattice direction of motion is up to 85° away from the applied Lorentz force direction.

Recently, e-beam writing based nanolithography¹ has been used to prepare submicrometric structures with geometries defined at will. In particular, the fabrication of superconducting thin films with periodic arrays of magnetic or non-magnetic dots^{2,3}, lines⁴, or holes⁵, with sizes comparable to characteristic lengths that govern superconductivity (the coherence length ξ and the penetration depth λ), opened the door to studies of static and dynamic properties of vortex matter. One of the most remarkable phenomena observed in samples with periodic arrays of defects is the commensurability effect in magnetoresistance and critical current²⁻¹⁴, which show that the vortex-lattice is strongly pinned at applied fields for which geometric matching exists between the vortex-lattice and the underlying periodic structure.

Vortex-lattice dynamics as a function of Lorentz force direction in this kind of samples has been investigated both theoretically^{15,16} and experimentally¹⁷ only for two privileged directions recently. In Nb thin films with rectangular arrays of magnetic dots¹⁷, the vortex motion is easier when the Lorentz force is applied parallel to the short than the long side of the rectangular array. This effect was related to channeled potential barriers for vortex motion in the shortest inter-dot distance direction.

In the present work, we have studied vortex–lattice dynamics as a function of the Lorentz force direction with respect to the array axes, in samples with rectangular array symmetries. For this purpose, we have developed experiments in which the direction of the Lorentz force is rotated any angle at will. We have found that the vortex-lattice is guided by channeled potentials along the short side of the array even though Lorentz force is applied up to 85° away of the short side of the rectangular array.

Arrays of submicrometric Ni dots on Si (100) substrates were fabricated using e-beam lithography techniques. Briefly, the pattern is defined by e-beam writing on the resist covering the substrate, followed by developing, and Ni sputter deposition. After lift-off only the Ni nanostructures remain on top of the substrate, which is then covered by a sputtered Nb thin film. Further details on this procedure can be found elsewhere¹.

Two arrays with rectangular symmetry but different periods $a \times b$ were used; sample A with $400 \times 625 \text{ nm}^2$ unit cell and sample B with $400 \times 500 \text{ nm}^2$ unit cell. On both samples, the dots are 40 nm high (Ni thickness) and their diameter is $\varnothing=250 \text{ nm}$. The Nb film on top of dot arrays is 100 nm thick.

For magnetotransport measurements, a cross-shaped bridge, designed for these rotating Lorentz force experiments, was optically lithographed and ion-etched. A sketch of the bridge, as well as notation and definition of angles and directions is shown in Figs. 1 (a) and (b). The two injected dc currents J_x and J_y cross in a square area containing the dot arrays. Taking into account Lorentz force expression, $\vec{F}_L = \vec{J} \times \vec{n} \phi_0$ (where $\phi_0 = 2.07 \cdot 10^{-15} \text{ Wb}$ and \vec{n} is a unitary vector parallel to the applied magnetic field), J_x and J_y yield two components of the Lorentz force on the vortex lattice, $F_x = J_y \phi_0$ and $F_y = J_x \phi_0$. Thus, the resultant Lorentz force, of magnitude $F_L = \sqrt{F_x^2 + F_y^2}$ and direction $\theta = \arctan(J_y/J_x)$, is selected at will, and it can be rotated in-plane in the whole angular range $0-90^\circ$, being parallel to the short lattice parameter a when $\theta = 0^\circ$ and to the long one b for $\theta = 90^\circ$. Voltage drops $V_x = V_2 - V_3$ and $V_y = V_1 - V_2$ were simultaneously measured using two nanovoltmeters. Experiments were carried out in a liquid He cryostat, provided with a superconducting magnet. In all measurements, the magnetic field was

always applied perpendicular to film plane, and thus perpendicular to the applied currents J_x and J_y .

Normal state ($T=9.5$ K) voltage drops V_x and V_y as a function of $\theta = \arctan(J_y/J_x)$ (Fig. 1 (c)) show sinusoidal behavior, proving that voltage contacts are well aligned. Superconducting critical temperatures T_c 's were independent of the measuring voltage contacts. For sample A it was $T_c=8.75$ K, and for sample B $T_c=8.63$ K, close to the $T_c=9.2$ K for bulk Nb.

The resistance along the x direction (long side b of rectangular array) $R_x = V_x/I_x$ versus applied field H is shown in Fig. 2 for different angles θ and fixed magnitude of the Lorentz force F_L , for samples A and B. For both samples, minima develop as a consequence of geometrical matching between vortex-lattice and the underlying periodic structure². For sample A two different periods ΔH are observed: at low fields $\Delta H_{low}=84$ Oe, whilst at higher fields $\Delta H_{high}=130$ Oe. The low-field period corresponds to fields at which an integer number of vortices exists per unit cell of the array, giving $\Delta H_{low} = \phi_0/ab = 82.9$ Oe, where $a=625$ nm and $b=400$ nm are dots array cell dimensions. The high-field period corresponds to $\Delta H_{high} = \phi_0/a^2 = 129$ Oe. The transition between these two different regimes has been explained in terms of the reconfiguration in the vortex lattice from rectangular to square geometry¹⁸. For sample B ($a=500$ nm and $b=400$ nm), this phenomenon is also observed, with a longer period $\Delta H_{high}=122$ Oe than the low field regime $\Delta H_{low}=104$ Oe, in good agreement with theoretical values $\Delta H_{low} = \phi_0/ab = 103$ Oe and $\Delta H_{high} = \phi_0/a^2 = 129$ Oe. In addition, fractional matching effects¹⁴ are observed for sample B, at fields $0.5\Delta H_{low}=52$ and $1.5\Delta H_{low}=156$ Oe. None of these features depend on

the direction of the Lorentz force, i.e. the position and period of matching fields do not change when Lorentz force is rotated at different angles θ . However, for both samples, the background resistance in the low field regime clearly depends on Lorentz force direction, and becomes lower as it is rotated towards the long side of the rectangular array b ($\theta \rightarrow 90$). At higher fields, the resistance becomes the same for all angles θ . This behavior clearly shows an anisotropic in-plane vortex dynamics.

Fig. 3 shows a different set of $R(H)$ for samples A and B, with $R_x = V_x/I_x$ and $R_y = V_y/I_y$ measured simultaneously. In these measurements, the current density J_x is kept constant, whilst J_y is changed for each curve. As a result, the Lorentz force F_y along the short side of the array a is kept constant, and the force F_x along the long side b is increased, thus resulting in a total variable Lorentz force $F_L = \sqrt{F_x^2 + F_y^2}$ with direction $\theta = \arctan(J_y/J_x)$. The behavior of both A and B samples is essentially the same (Fig. 3). For fields up to the first matching and $\theta < 85^\circ$, R_x is independent of F_x . Moreover, in these field range, R_y falls below measurable values, much lower than R_x ; that is $V_y \ll V_x$, indicating that vortex lattice is essentially moving along the short side a of the array. It is worth noting that vortex-lattice motion is confined along the short side a of the array, even though the total Lorentz force F_L is rotated up to $\theta=85^\circ$, very close to the direction of the long side of the array b . For fields higher than the first matching, a measurable resistance R_y progressively arises. Thus, the vortex-lattice direction of motion no longer is restricted to the a direction, but it rotates as magnetic field increases, becoming parallel to the direction of the applied Lorentz force F_L .

The phenomenology described above constitutes the central result of this paper. The anisotropic pinning potential due to the rectangular array of magnetic dots¹⁷ creates a hard-

axis, along the short side b , for vortex-lattice motion. The important point is that this effect is strong enough to lock vortex motion along the short side a of the rectangle. Vortex-lattice motion is guided along this direction for fields up to the first matching field, disappearing progressively for more intense fields; as the number of weakly pinned interstitial vortices² increases the guided vortices effect is reduced.

To gain further insight into this anisotropic vortex-lattice dynamics, I-V curves (not shown) were measured at $T=0.99T_c$ for several $\theta = \arctan(J_y/J_x)$ at different applied fields. The vortex-lattice velocities along the x (hard) and y (easy) axes are calculated from the voltage drops V_x and V_y , using $v_i = V_i/(dB)$, where d is the distance between contacts and B the applied field. Here we used that the vortex-lattice velocity $v = \sqrt{v_x^2 + v_y^2}$ gives the electric field $\vec{E} = \vec{B} \times \vec{v}$. Together with the Lorentz force expression, $F_L = \sqrt{F_x^2 + F_y^2}$, we can derive F_L - v curves from I-V characteristics. This is interesting since¹⁹ a comparison of the Lorentz force necessary to drive the vortex-lattice with a velocity v at out-of-matching field (F_{Lout}) with that at matching ($F_{Lmatching}$), gives the effective force at matching (ΔF_L) as a function of velocity,

$$F_{Lmatching}(v) - F_{Lout}(v) \equiv \Delta F_L(v)$$

This analysis for the first matching field is shown in Fig. 4, for sample A ($H_{out}=45$ Oe, $H_{matching}=84$ Oe) and B ($H_{out}=70$ Oe, $H_{matching}=104$). Figs. 4 (a) and (b) show that, for angles up to $\theta = 60^\circ$, the maxima of the effective force are for velocities around 200 m/s in both samples, well in the range earlier reported¹⁹, and, most important, do not depend on the direction of the Lorentz force. However, as Lorentz force direction approaches the hard-axis b ($60 < \theta \rightarrow 90$, perpendicular to the channel direction), the maxima shift

towards lower velocities. On the other hand, $\Delta F_L(\theta)$ increases monotonically for all θ . Figs. 4 (c) and (d) show $\Delta F_L(\theta) \times \cos(\theta)$. $\Delta F_L(\theta) \times \cos(\theta) \approx \Delta F_L(\theta = 0)$ up to a given velocity, which depends on sample anisotropy and Lorentz force direction (θ). This clarifies the behavior observed in Figs. 4 (a) and (b). Up to a given vortex-lattice velocity, dependent on Lorentz force direction, only the F_y component (along easy-axis a) plays a role in vortex dynamics. In agreement with the picture described above, the vortex motion is restricted to this direction for fields up to first matching field. The component of the Lorentz force along the hard-axis b , F_x , has no effect until a threshold for vortex-lattice velocity is reached. For both samples, this threshold is lower as the direction of the Lorentz force is closer to the hard-axis (see arrows in Figs. 4 (a) and (b)). The more anisotropic is the rectangular array (sample A), the higher the threshold velocity for each Lorentz force direction.

In conclusion, measurement of the vortex-lattice velocity v versus applied Lorentz force F_L shows that, up to a given vortex-lattice velocity threshold, the vortex motion in rectangular pinning arrays is strongly guided by the microstructure along the short side of the array. The physical origin of this guided vortex motion is the channeling potential landscape created by the rectangular symmetry. This results in vortex-lattice velocity and Lorentz force not being parallel for fields up to the first matching minimum: the effect is strong enough to keep vortex-lattice motion up to 85° away from the Lorentz force direction., and only the component of the Lorentz force F_y along the short side of the array plays a role in vortex dynamics. The effect is tunable by the dots array anisotropy: the higher the anisotropy of the dot array, the wider the range of velocities in which the guided vortex motion occurs.

We acknowledge grant MAT02-04543 from Spanish CICYT, Fundación Ramón Areces, New Del Amo Program and ESF-VORTEX Program. Work at UCSD supported by the US-DOE. We thank Prof. J. Santamaría for useful conversations and critical reading of the manuscript, and thank A. Silhanek and J. Schuller for helpful conversations.

- ¹ J.I. Martín, J. Nogués, K. Liu, J.L. Vicent and I. K. Schuller, *J. Magn. Magn. Mat.* **256**, 449 (2002).
- ² J.I. Martín, M. Vélez, J. Nogués, and Ivan K. Schuller, *Phys. Rev. Lett.* **78**, 1929 (1997)
- ³ Y. Jaccard, J. I. Martín, M.-C. Cyrille, M. Vélez, J. L. Vicent, and I. K. Schuller *Phys. Rev. B* **58**, 8232 (1998).
- ⁴ D. Jaque, E. M. González, J. I. Martín, J. V. Anguita, and J. L. Vicent, *Appl. Phys. Lett.* **81**, 2851 (2002).
- ⁵ L. Van Look, B. Y. Zhu, R. Jonckheere, B. R. Zhao, Z. X. Zhao, and V. V. Moshchalkov, *Phys. Rev. B* **66**, 214511 (2002).
- ⁶ O. Daldini, P. Martinoli, J.L. Olsen, and G. Berner, *Phys. Rev. Lett.* **32**, 218 (1974).
- ⁷ A.T. Fiory, A.F. Hebard, and S. Somekh, *Appl. Phys. Lett.* **32**, 73 (1978).
- ⁸ A. Pruyboom, P.H. Kes, E. van der Drift, and S. Radelaar, *Phys. Rev. Lett.* **60**, 1430 (1988).
- ⁹ Y. Otani, B. Pannetier, J.P. Nozières, and D. Givord, *J. Magn. Magn. Mater.* **126**, 622 (1993).
- ¹⁰ M. Baert, V. Metlushko, R. Jonckheere, V.V. Moshchalkov, and Y. Bruynseraede, *Phys. Rev. Lett.* **74**, 3269 (1995).
- ¹¹ D.J. Morgan and J.B. Ketterson, *Phys. Rev. Lett.* **80**, 3614 (1998).
- ¹² V. Metlushko, U. Welp, G.W. Crabtree, R. Osgood, S.D. Bader, L.E. De Long, Z. Zhang, S.R.J. Brueck, B. Ilic, K. Chung, and P. Hesketh, *Phys. Rev. B* **60**, R12585 (1999).
- ¹³ Y. Fasano, J.A. Herbsommer, F. de la Cruz, F. Pardo, P. Gammel, E. Bucher, and D. Bishop, *Phys. Rev. B* **60**, R15047 (1999).

- ¹⁴ O. M. Stoll, M. I. Montero, J. Guimpel, J. J. Åkerman, and I. K. Schuller, Phys. Rev. B **65**, 104518 (2002).
- ¹⁵ C. Reichhardt and F. Nori, Phys. Rev. Lett. **82**, 414 (1999).
- ¹⁶ C. Reichhardt, G.T. Zimanyi, and N. Gronbech-Jensen, Phys.Rev. B **64**, 014501 (2001).
- ¹⁷ M. Velez, D. Jaque, J. I. Martín, M. I. Montero, I. K. Schuller, and J. L. Vicent, Phys. Rev. B **65**, 104511 (2002).
- ¹⁸ J. I. Martín, M. Vélez, A. Hoffmann, I. K. Schuller, and J. L. Vicent, Phys. Rev. Lett. **83**, 1022 (1999).
- ¹⁹ M. Vélez, D. Jaque, J. I. Martín, F. Guinea, and J. L. Vicent, Phys. Rev. B **65**, 094509 (2002).

FIGURE CAPTIONS

Figure 1: (a) Micrograph of the measurement bridge. The area in which currents cross is $40 \times 40 \mu\text{m}^2$. Shaded area represents the $90 \times 90 \mu\text{m}^2$ array of dots. (b) Definition of angle θ , and current and voltage directions with respect to array axes. (c) Voltage drops $V_y = V_1 - V_2$ and $V_x = V_2 - V_3$ as a function of θ above T_c ($T = 9.5 \text{ K}$), with $\sqrt{J_x^2 + J_y^2} = 10 \text{ kA cm}^{-2}$ (d) SEM image of the array of sample A ($a = 400 \text{ nm}$, $b = 625 \text{ nm}$).

Figure 2: (a) $R_x(H)$ vs. applied field of sample A for different angles θ and $\sqrt{J_x^2 + J_y^2} = 75 \text{ kA cm}^{-2}$ at $T = 0.98T_c$. Vertical dashed lines point out matching fields with period $\Delta H_{low} = 84 \text{ Oe}$, and dashed-dot lines those with $\Delta H_{high} = 130 \text{ Oe}$. (b) $R_x(H)$ vs. applied field of sample B for different angles θ and $\sqrt{J_x^2 + J_y^2} = 12.5 \text{ kA cm}^{-2}$ at $T = 0.99T_c$. Vertical dashed lines point out matching fields with period $\Delta H_{low} = 104 \text{ Oe}$, dashed-dotted lines those with $\Delta H_{high} = 122 \text{ Oe}$, and dotted lines mark fractional matching fields $0.5\Delta H_{low} = 52 \text{ Oe}$ and $1.5\Delta H_{low} = 156 \text{ Oe}$.

Figure 3: (a) $R_x(H)$ and (b) $R_y(H)$ of sample A at $T = 0.99T_c$, for $J_x = 25 \text{ kA cm}^{-2}$ and different J_y : (solid squares) $J_y = 0$ ($\theta = 0$), (circles) $J_y = 12.5 \text{ kA cm}^{-2}$ ($\theta = 30$), (solid up triangles) $J_y = 43.3 \text{ kA cm}^{-2}$ ($\theta = 60$) and (down triangles) $J_y = 68.8 \text{ kA cm}^{-2}$ ($\theta = 75$). (c) $R_x(H)$ and (d) $R_y(H)$ of sample B at $T = 0.99T_c$, for $J_x = 12.5 \text{ kA cm}^{-2}$ and different J_y : (solid squares) $J_y = 0$ ($\theta = 0$), (circles) $J_y = 7.25 \text{ kA cm}^{-2}$ ($\theta = 30$), (solid up triangles) $J_y = 12.5 \text{ kA cm}^{-2}$ ($\theta = 45$), (up triangles) $J_y = 21.6 \text{ kA cm}^{-2}$ ($\theta = 60$), (solid diamonds) $J_y = 34.3 \text{ kA cm}^{-2}$ ($\theta = 70$) and (left triangles) $J_y = 142.2 \text{ kA cm}^{-2}$ ($\theta = 85$). Dashed line points out first matching fields.

Figure 4: (a) $\Delta F_L(v)$ for sample B around first matching, for different directions of the Lorentz force (see legend). (b) $\Delta F_L(v)$ for sample A around first matching, for different directions of the Lorentz force (see legend). (c) $\Delta F_L(v) \times \cos(\theta)$ for sample B around first matching (see legend). (d) $\Delta F_L(v) \times \cos(\theta)$ for sample A around first matching (see legend). Horizontal arrows in (c) and (d) point out vortex velocity threshold for guided vortex motion.

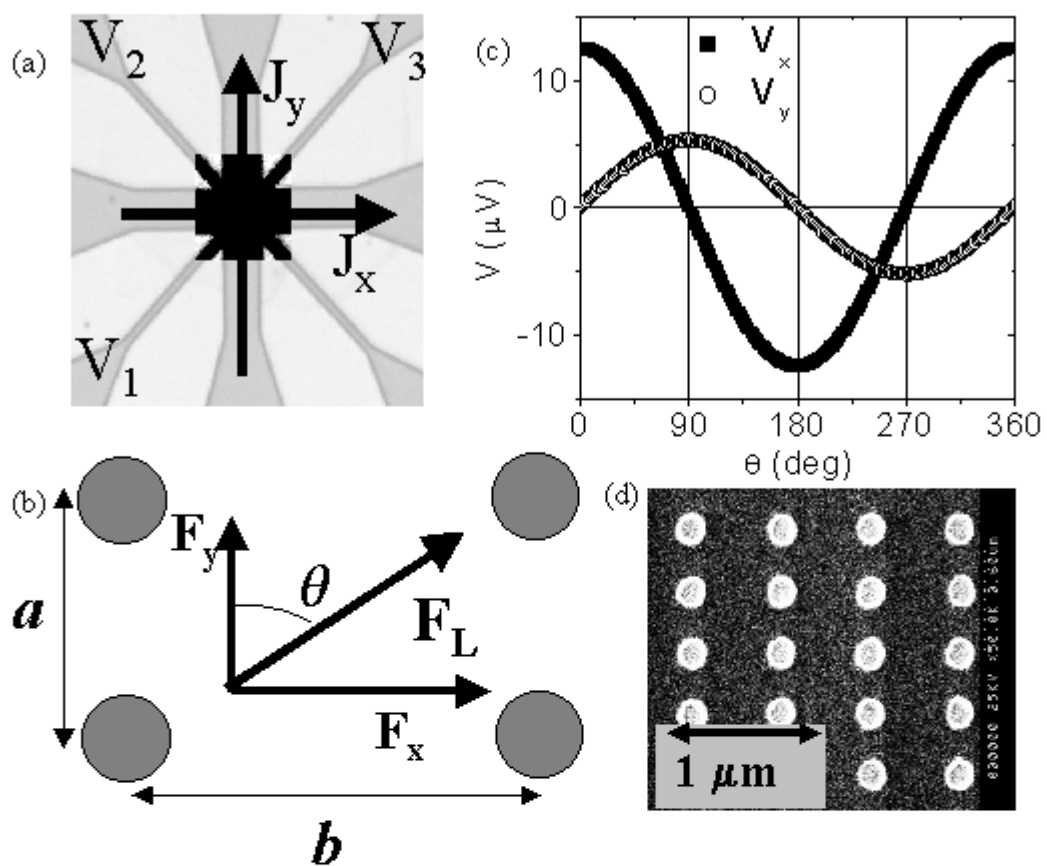


Figure 1
J.E. Villegas *et al.*

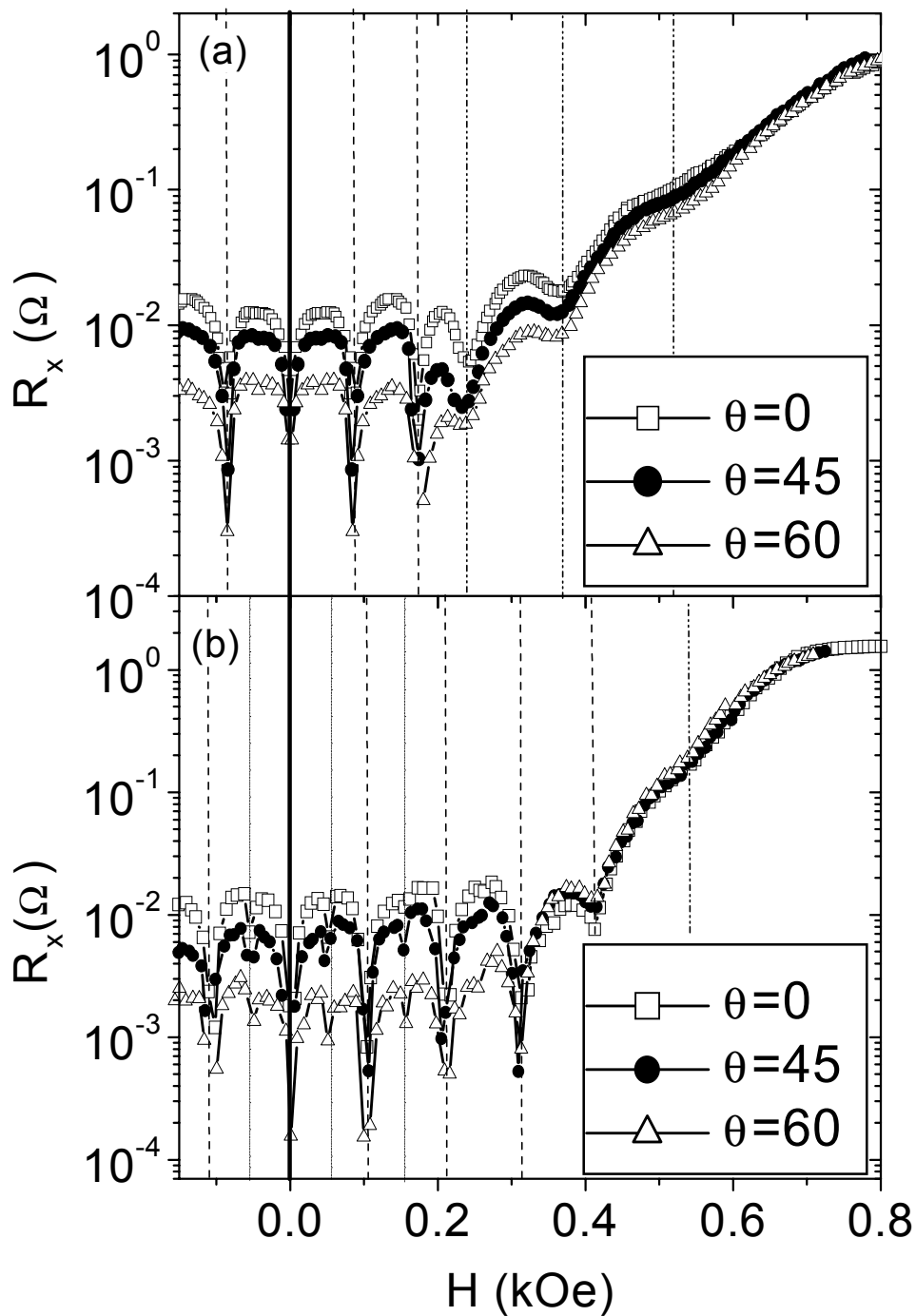


Figure 2
J.E. Villegas *et al.*

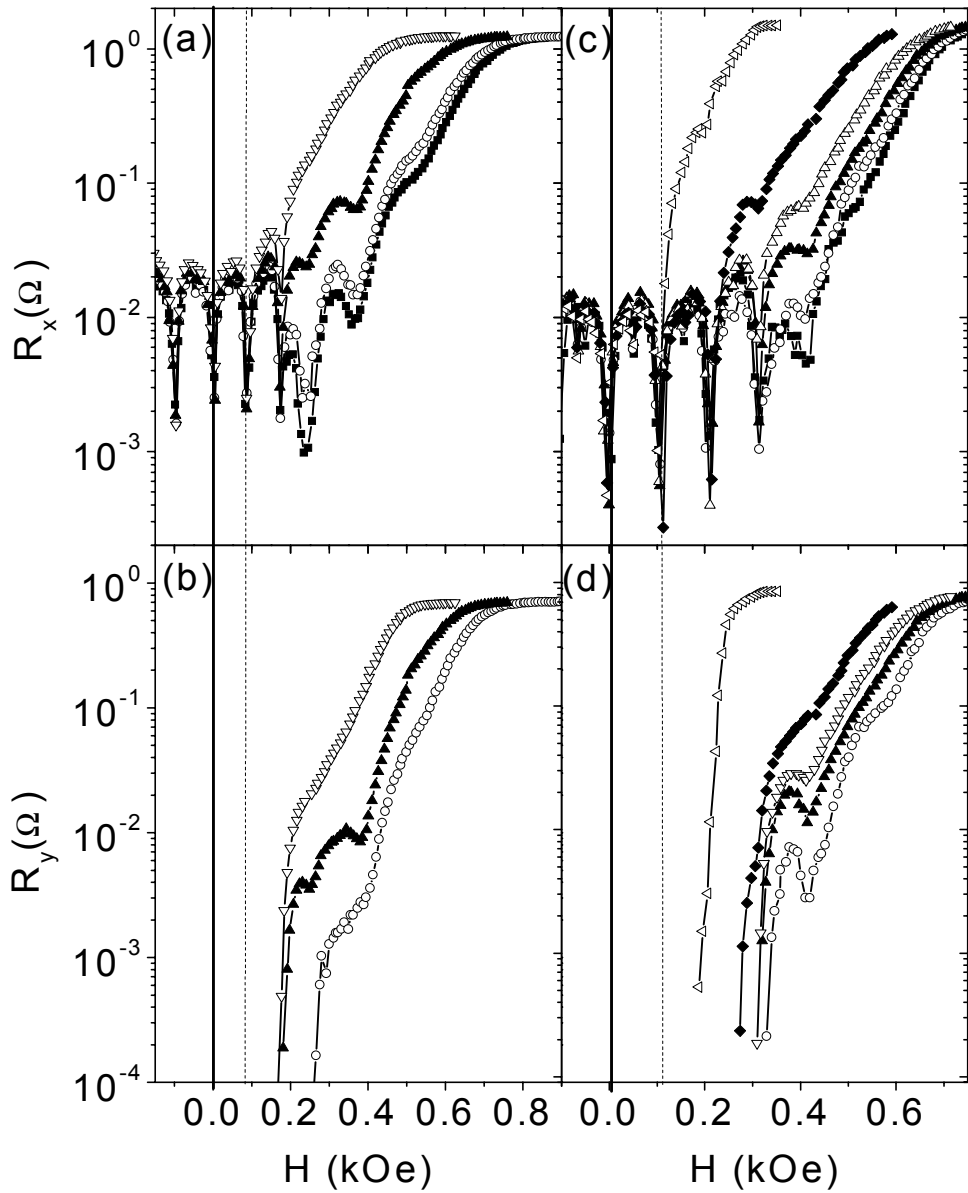


Figure 3
J.E. Villegas *et al.*

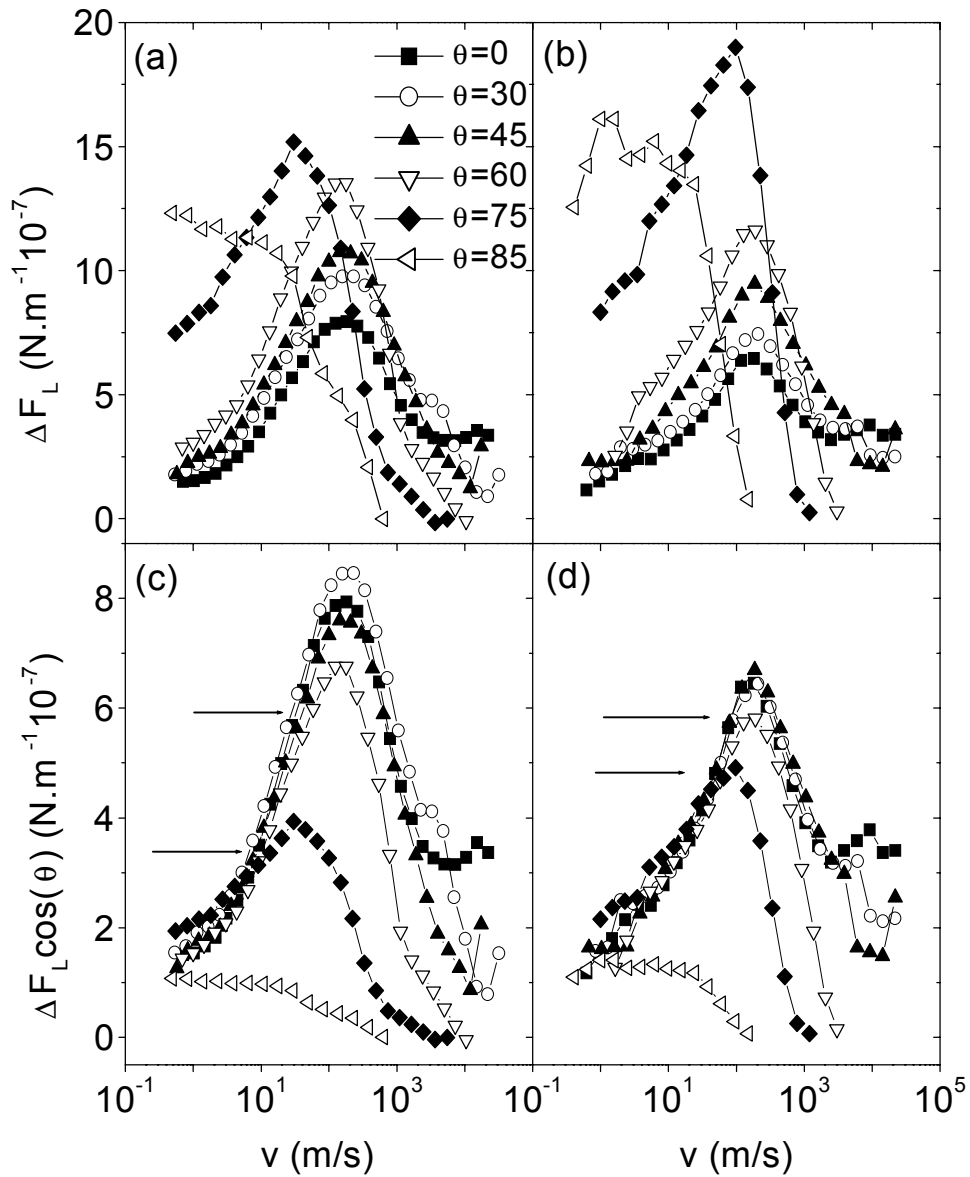


Figure 4
J.E. Villegas *et al.*